

Current status and progress of laser-plasma experiments

Alexander Sävert

Helmholtz Institute Jena

EMMI Physics Day 2023

Electron beams for bright x-ray sources



Eu XFEL Hamburg since 2017, total length 3.4 km, cost ca. 1 B€
(1.7 km superconducting accelerator, maximum energy: 17.5 GeV)

Down sizing electron accelerators

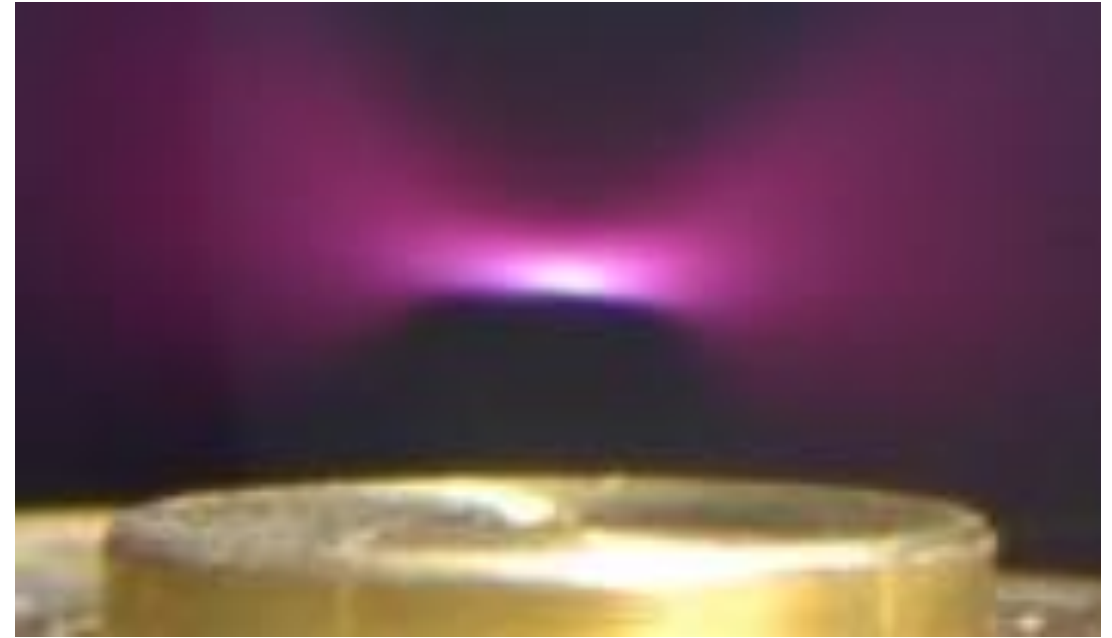
1.25 m



Superconducting rf- cavity

Electric fields: 30 MV/m

1.25 cm



Plasma target

Electric fields: 300 GV/m @ $n_e = 1 \times 10^{19} \text{ cm}^{-3}$

The Laser Wake Field Accelerator

VOLUME 43, NUMBER 4

PHYSICAL REVIEW LETTERS

23 JULY 1979

Laser Electron Accelerator

T. Tajima and J. M. Dawson

Department of Physics, University of California, Los Angeles, California 90024

(Received 9 March 1979)

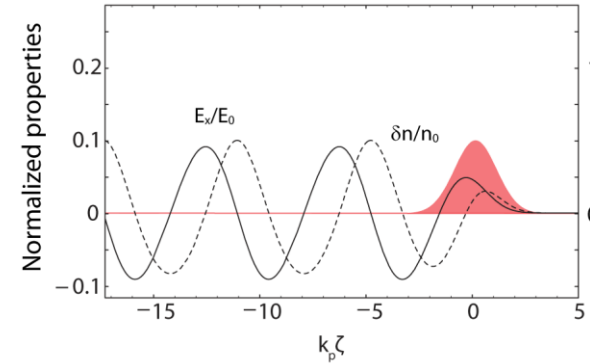
An intense electromagnetic pulse can create a weak of plasma oscillations through the action of the nonlinear ponderomotive force. Electrons trapped in the wake can be accelerated to high energy. Existing glass lasers of power density $10^{18}\text{W}/\text{cm}^2$ shone on plasmas of densities 10^{18} cm^{-3} can yield gigaelectronvolts of electron energy per centimeter of acceleration distance. This acceleration mechanism is demonstrated through computer simulation. Applications to accelerators and pulsers are examined.

$$\text{Ponderomotive force: } \vec{F}_{pond} = -\frac{e^2}{4\langle\gamma\rangle m_e \omega_0^2} \nabla \vec{E}^2$$

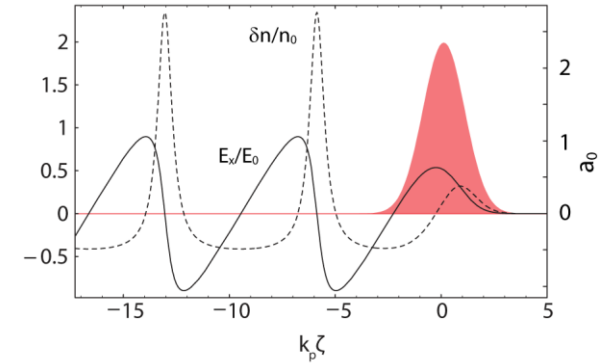
$$\text{normalized vector potential: } a_0 = \frac{eE_0}{m_e c \omega_p}$$

$$\text{plasma frequency: } \omega_p = \sqrt{\frac{e^2 n_e}{\epsilon_0 m_e}}$$

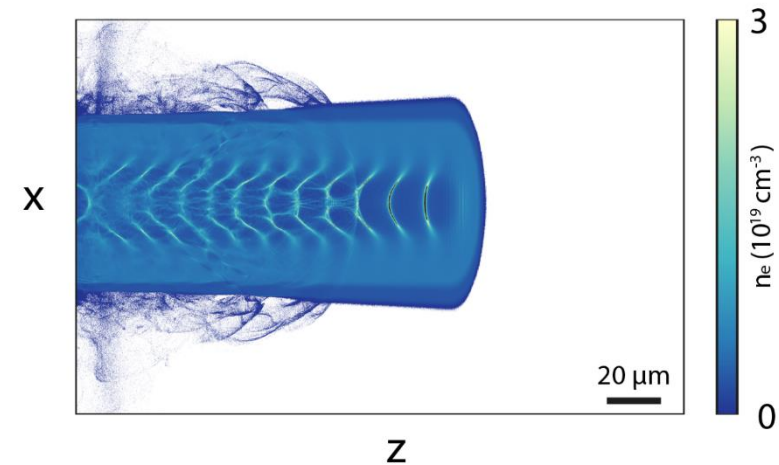
1D: weak excitation



strong excitation



2D:



JENA

Helmholtz Institute Jena

High intensity lasers @ Helmholtz Institute Jena

JETi ONE



Wavelength: 0,8-7 μm
Energy on target: 0,5 mJ
Pulse duration: few cycle
Peak power: -
Repetition rate: 1 kHz

JETi200



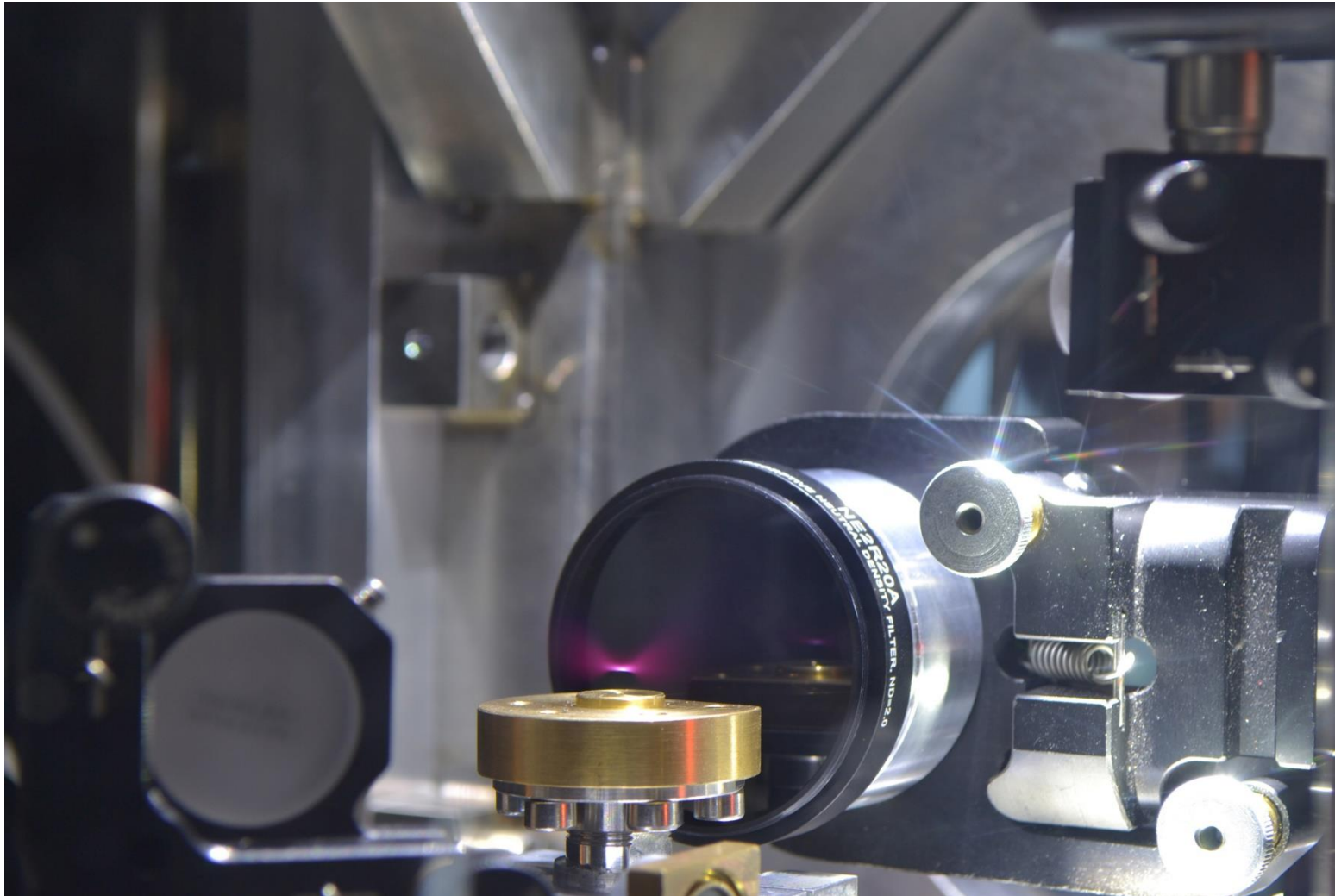
Wavelength: 800 nm
Energy on target: 5 J
Pulse duration: 17 fs
Peak power: 300 TW
Repetition rate: 5 Hz

POLARIS

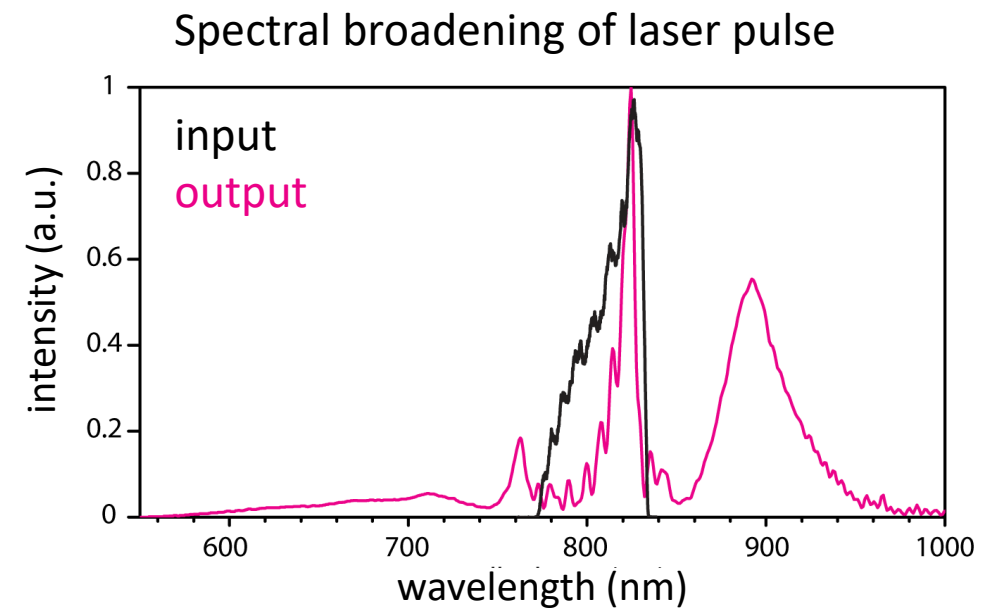
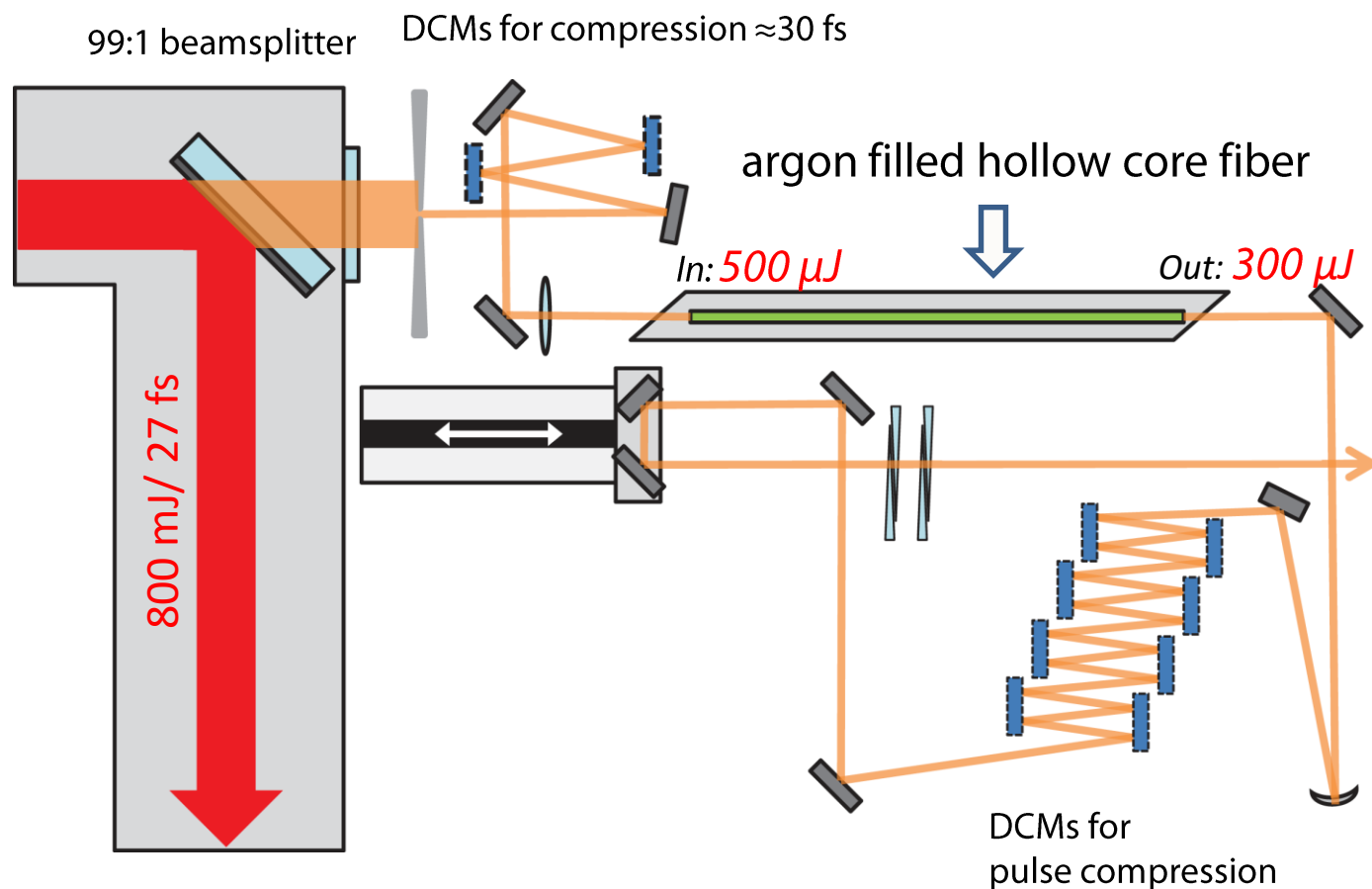


Wavelength: 1030 nm
Energy on target: 16 J (54 J)
Pulse duration: 100 fs
Peak power: 160 TW
Repetition rate: 1/50 Hz

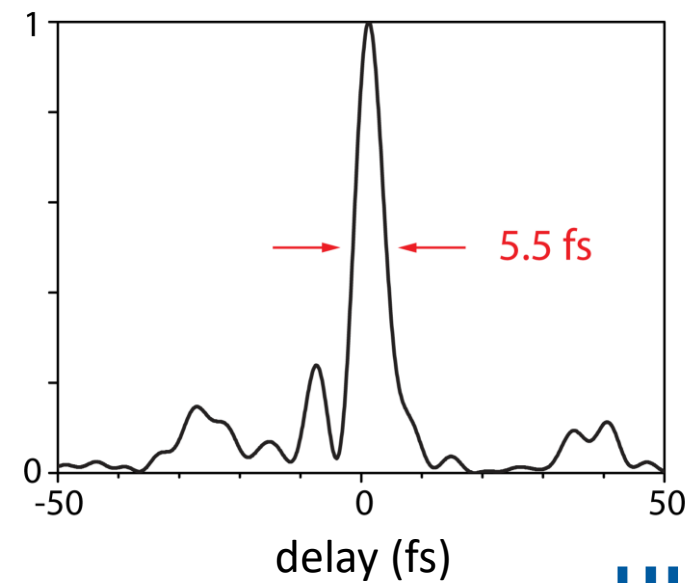
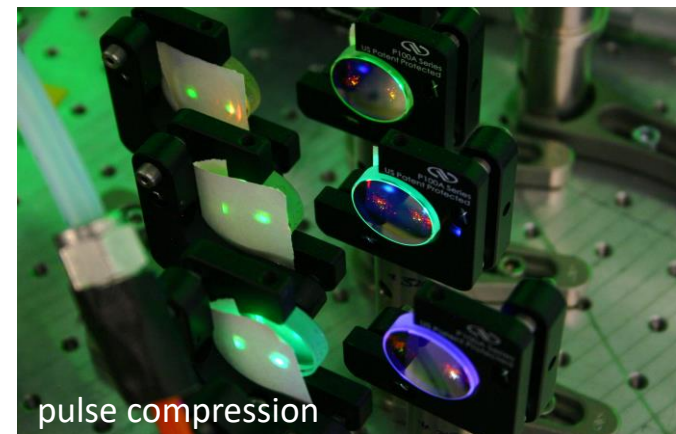
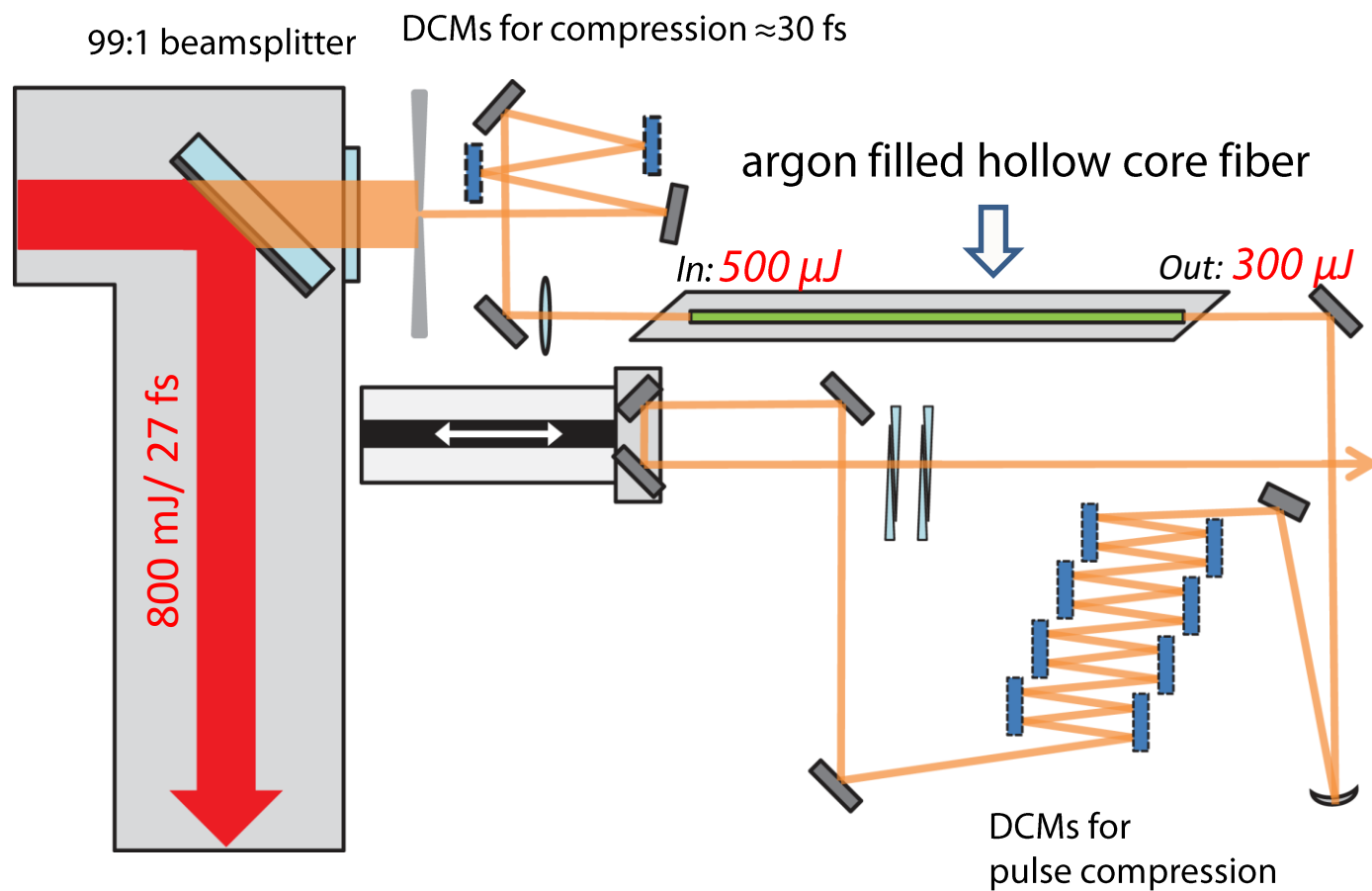
Typical Laser Wakefield Acceleration setup



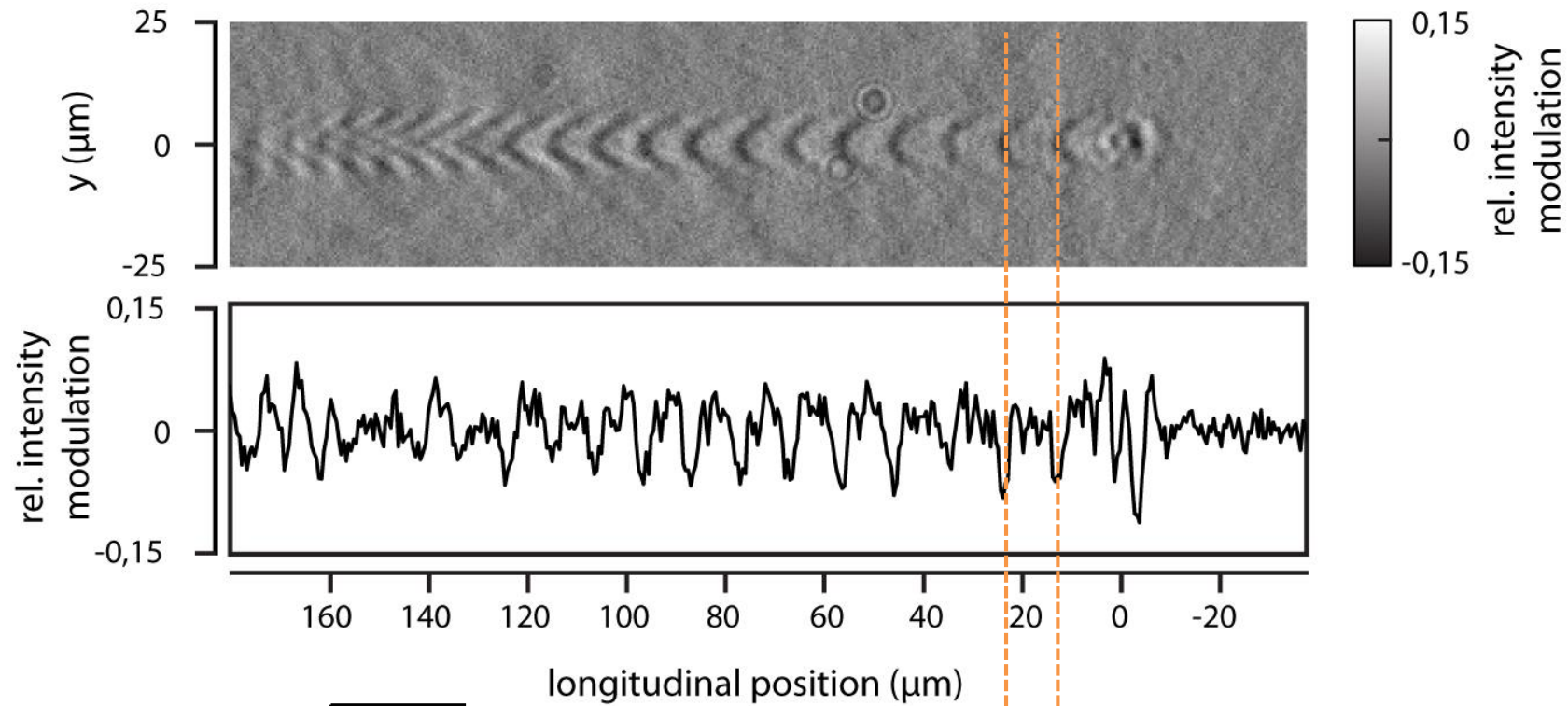
Few cycle probe beam - setup



Few cycle probe beam - setup



Shadowgraphy with 6 fs probe pulses

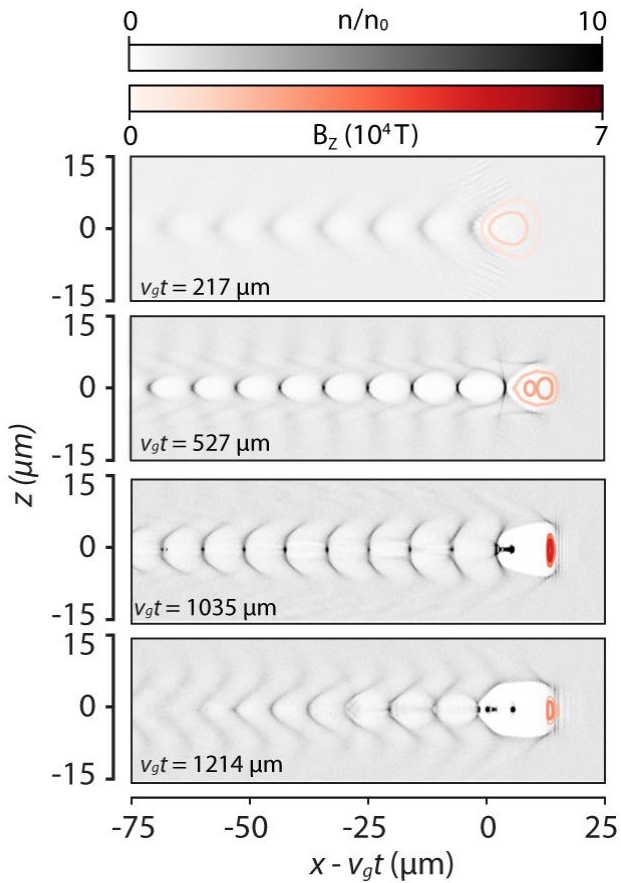


Plasma wavelength $\lambda_p = 2\pi c \sqrt{\frac{\epsilon_0 m_e}{n_e e^2}}$

$\lambda_p = 10.8 \mu m$

Injection mechanisms

Changes in bubble geometry



Bubble elongation leads to injection

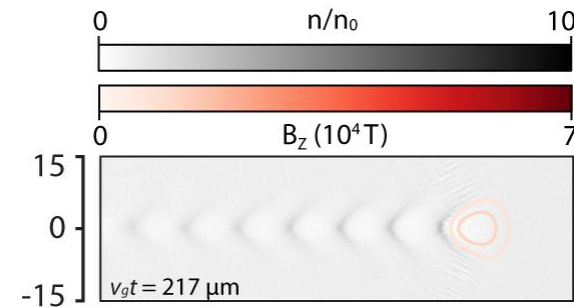
Self injection: Increase in peak intensity by self focusing and pulse shortening

Density downramp: Slow change in electron density

Shockfront: Sharp change in electron density

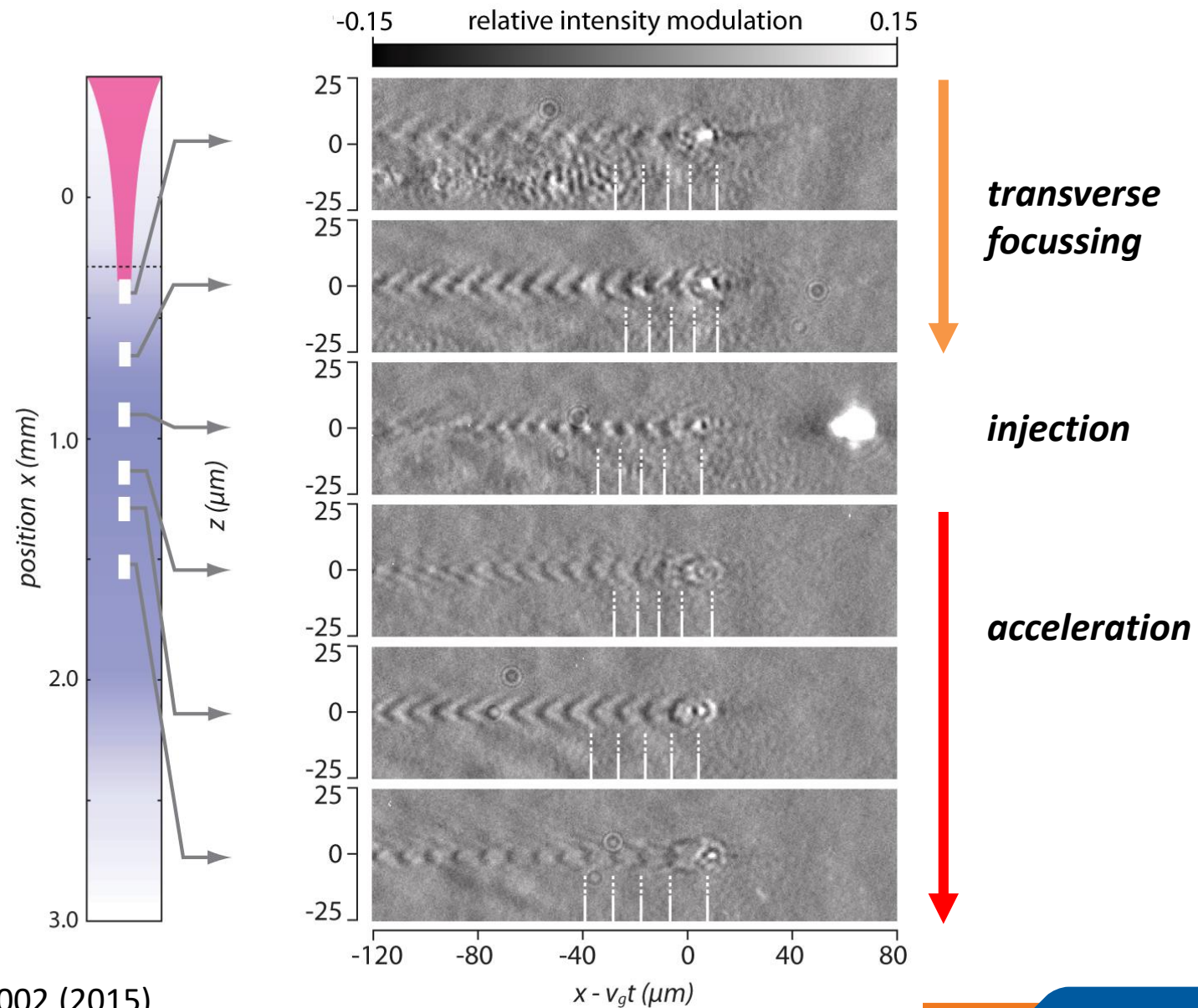
$$\lambda_p = 2\pi c \sqrt{\frac{\epsilon_0 m_e}{n_e e^2}}$$

Ionization injection



Secondary ion species with higher inner core ionization threshold (e.g Nitrogen 552 eV/667 eV)

Evolution of the plasma wakefield

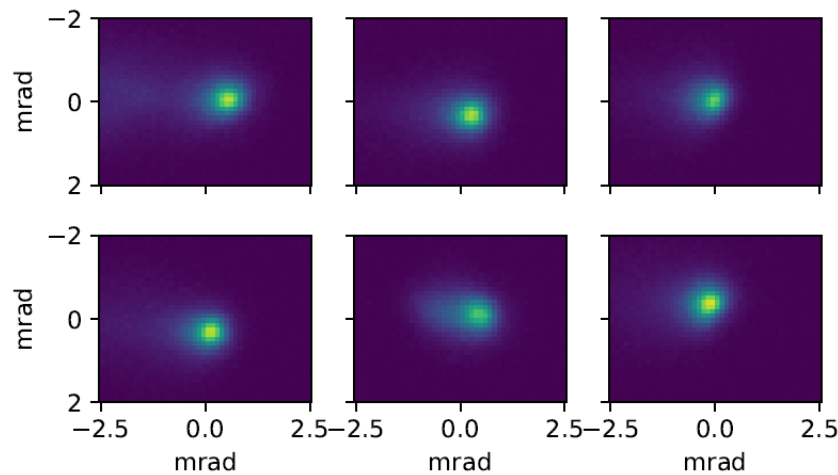
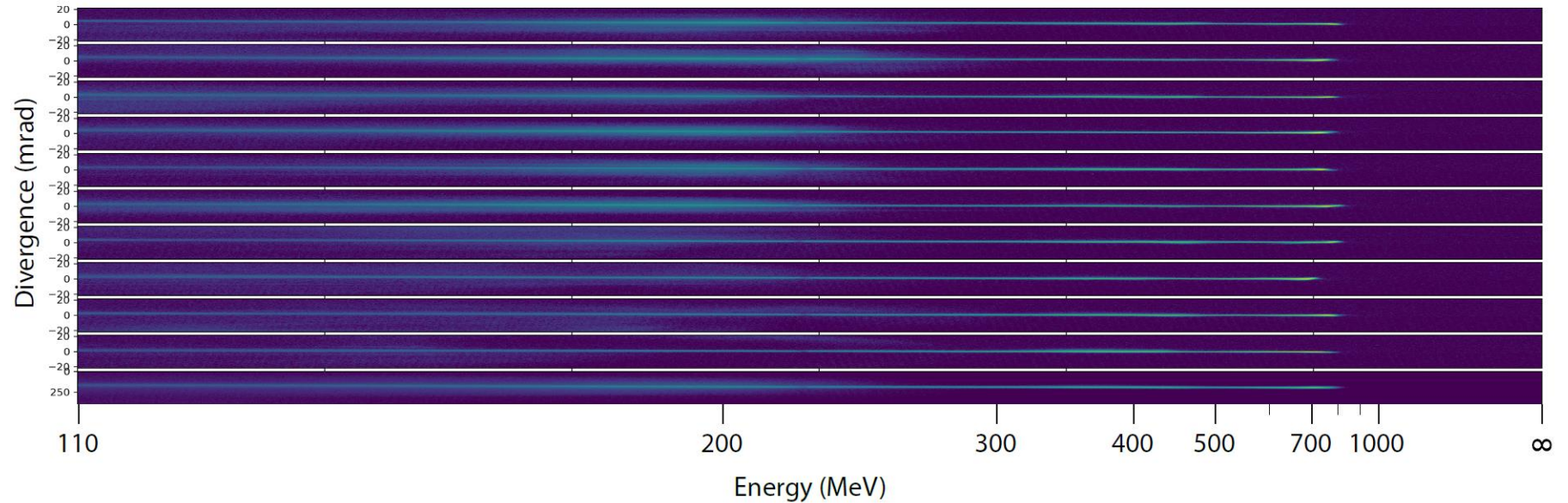


Electron acceleration to the GeV level



- home made gas cell with variable length

LWFA with ionization injection (95% He, 5% N₂)



- GeV beams with ultra low beam divergence $< 0.5 \text{ mrad}^2$
- pointing fluctuations on same order as divergence
- new target design for bandwidth control

Bayesian optimization of a Laser-Plasma Accelerator

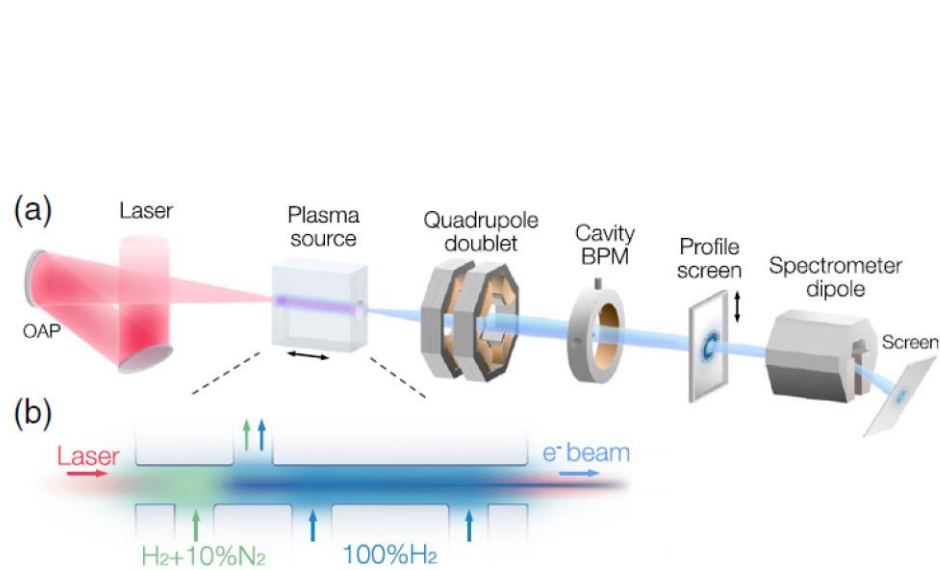


FIG. 1. Laser-plasma accelerator. (a) Schematic of the LUX laser and electron beam line. (b) Structured plasma source supplied with H₂ and doped with 10% N₂ in the front for controlled injection of electron bunches into the laser-driven plasma wave.

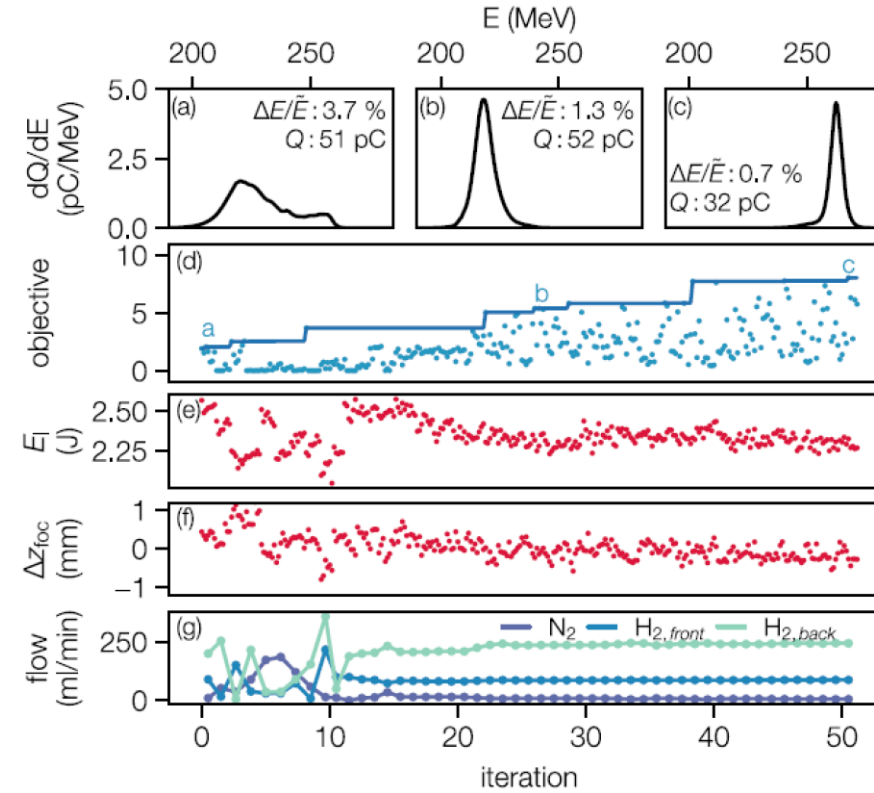


FIG. 3. Experimental optimization of LPA electron beams: (a)–(c) Measured energy spectra; (d) measured objective function (dots) with the cumulative best result (blue line); (e)–(g) Input parameters with shot to shot measurements of the laser energy, focus position, and gas flows for each input setting.

Long term stability of an LWFA

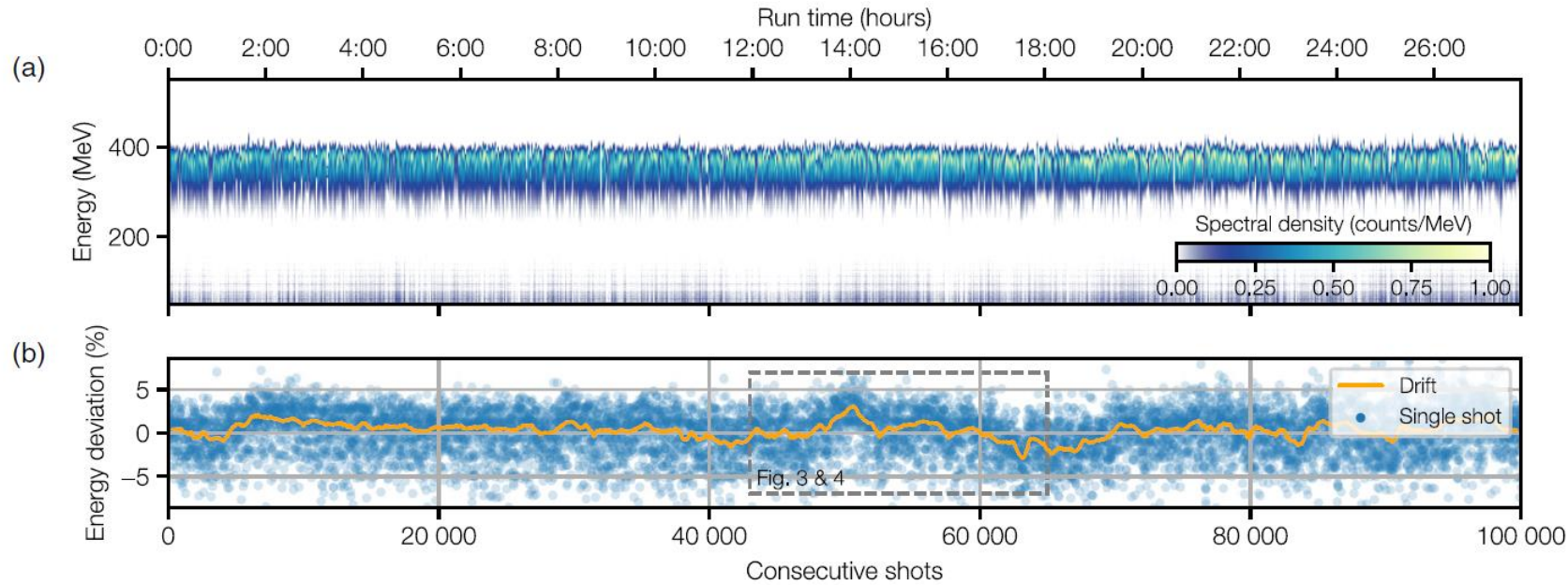


FIG. 2. Panel (a) shows the energy spectra of 100 000 consecutive laser-plasma generated electron beams. Here, each line represents one single shot. The camera images of the electron spectrometer screen are background corrected, projected onto the dispersive axis, and calibrated to a linear energy scale. The peak energy of each spectrum (dots) is shown in panel (b), together with the energy drift (solid line) calculated as the rolling average over a 6-min window, i.e., 360 shots. The percent-level energy drift can be attributed to a drift in drive laser parameters (compare Figs. 3 and 4).

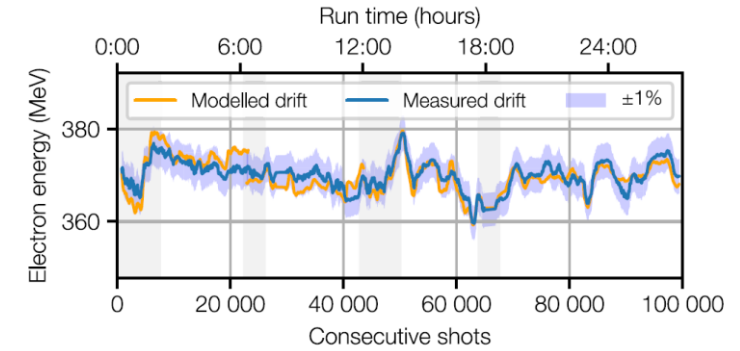
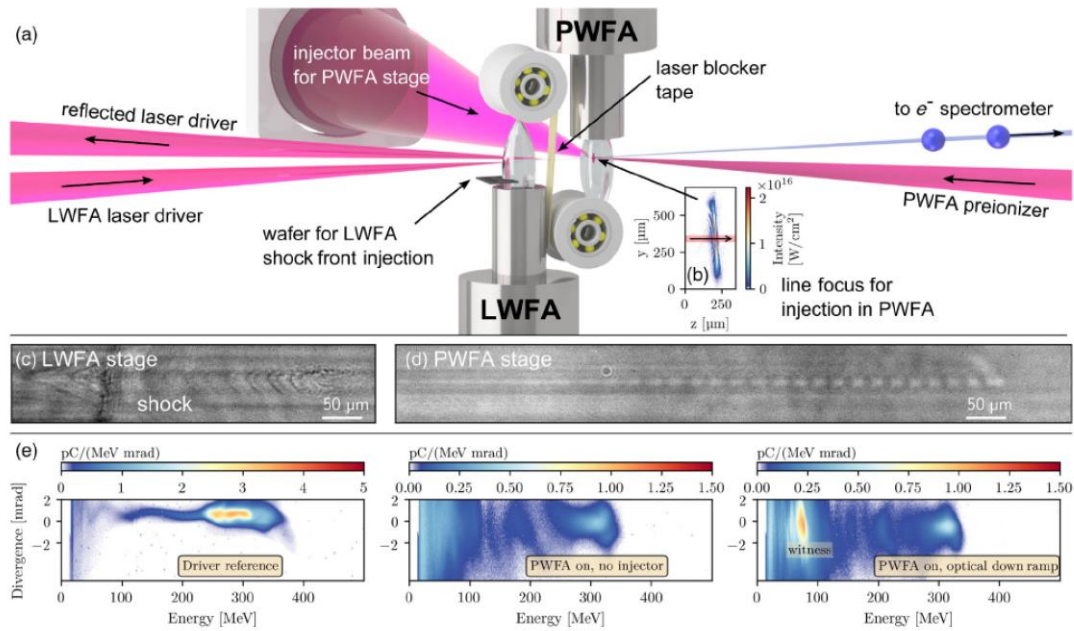


FIG. 5. Gray shaded areas mark the events used to derive the correlations $\partial_E \mathcal{E}$, $\partial_Z \mathcal{E}$, and $\partial_\theta \mathcal{E}$. By regularly updating the correlations, the parametrization of the electron energy drift can be extended to the full data set.

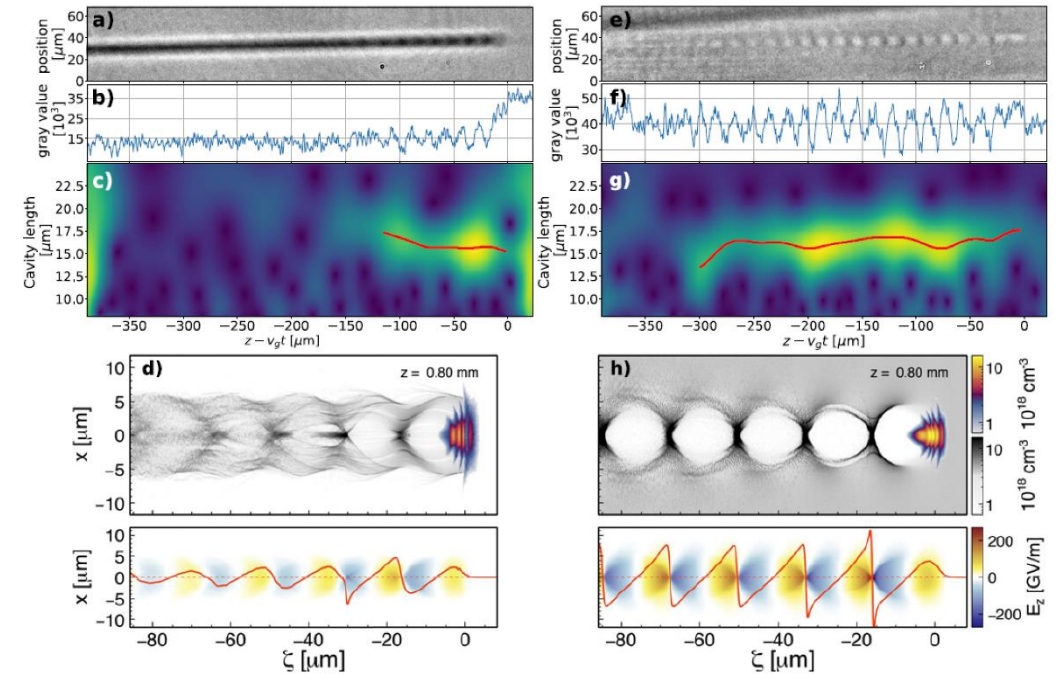
Few Cycle Microscopy for Particle Wakefield Acceleration



M. Förster et al. *PhysRevX*. **12**, 041016 (2022)

without pre ionization

with pre ionization



S. Schöbel et al. *NewJPhys*. **24**, 083034 (2022)

Major breakthroughs in LWFA

Free-electron lasing at 27 nanometres based on a laser wakefield accelerator

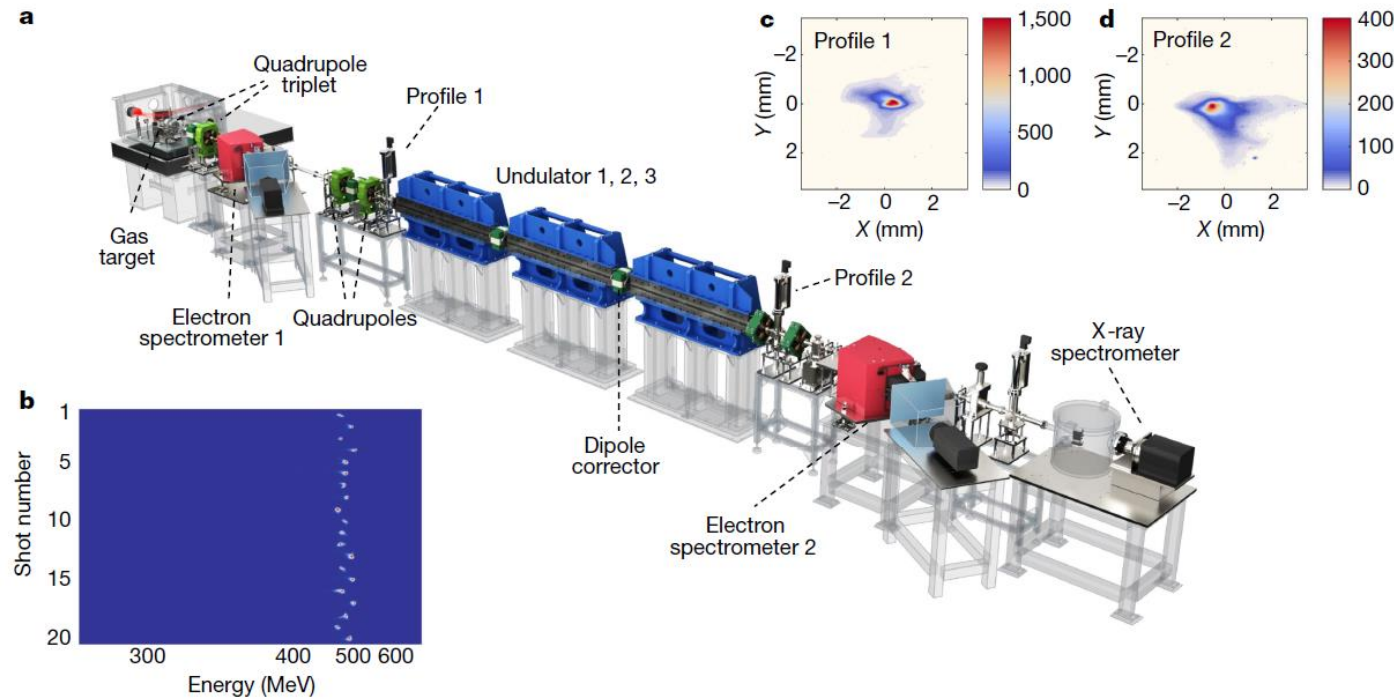
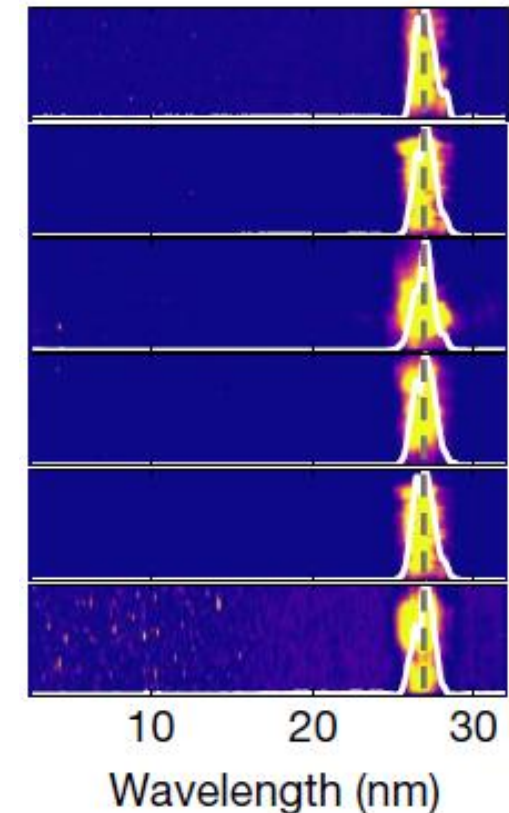


Fig. 1 | Schematic layout of LWFA-based free electron laser experiment. **a**, Undulator beamline with a total length of approximately 12 m from the gas target for the LWFA to the X-ray spectrometer. **b**, Typical spectra of electron

beams from the LWFA for 20 consecutive shots. **c**, **d**, Measured transverse profiles of the electron beam at the entrance (**c**) and exit (**d**) of the undulators. The scale bars are normalized.

radiation spectra



Electron bunch parameter: 490 MeV, 0.5 % energy spread, 30 pC, 5-10 kA

Seeded free-electron laser driven by a compact laser plasma accelerator

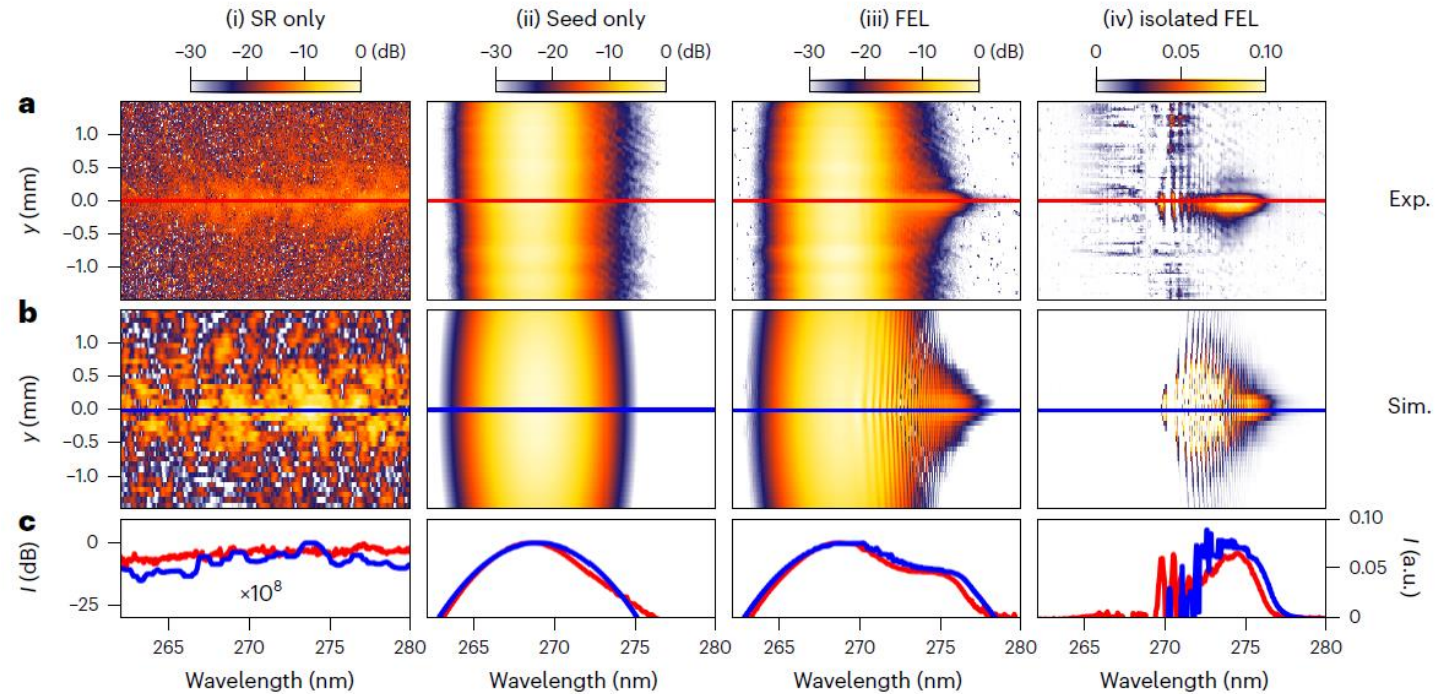


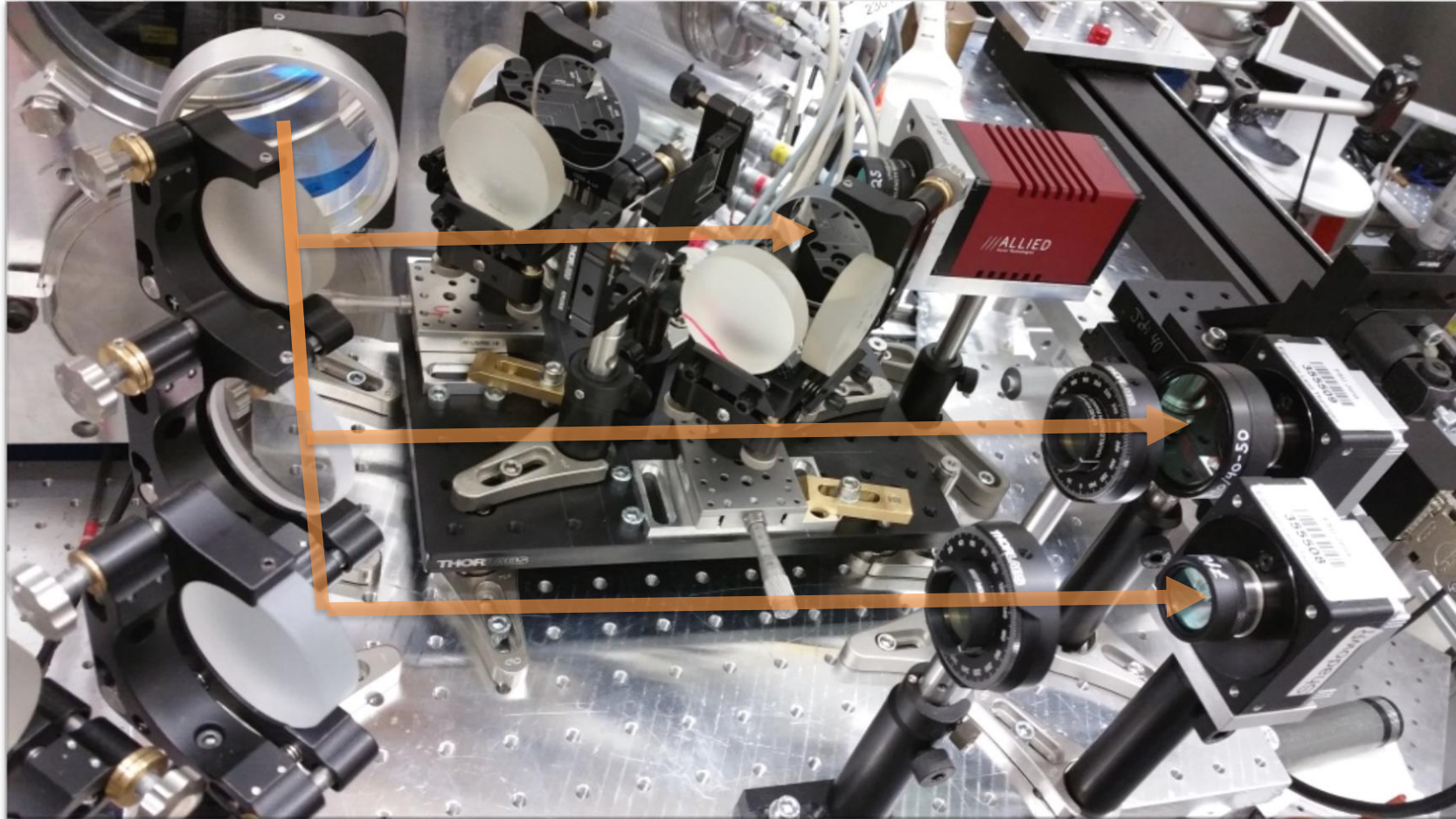
Fig. 2 | Spatio-spectral distributions of the radiation at the undulator exit. **a,b**, Spatio-spectral distributions for an undulator gap of 4.3 mm ($K_u = 2.35$) and an optimum delay of +0.1 ps: experimental measurements (**a**) and simulation (**b**) of SR only (i), seed only (ii), SR with seed (iii) and the difference between the (iii) and (ii) images (iv). **c**, On-axis spectral intensity I extracted along the red line in **a** and blue line in **b** with integration over $\Delta y = 0.3$ mm and median filtering of the simulated profile. In **a,b,c(i-iii)**, distributions are normalized to their maximum

intensity and displayed in logarithmic (dB) scale. In **a,b,c(iv)**, the distributions are displayed in a linear scale. Simulation parameters (electron-beam parameters given at the source point): $E_e = 188.8$ MeV, charge = 150 pC, $\sigma_z = 2$ μ m (r.m.s.), normalized emittance $\epsilon_{x,y} = (1.5; 1.0)$ mm mrad, divergence $\sigma_{x',y'} = (1.5; 1.0)$ mrad (r.m.s.), $\sigma_e = 5\%$ (r.m.s.), $R_{56} = -1.8$ mm, QUAPEVA 2 strength detuned by -2% , $E_{seed} = 0.5$ μ J, $\lambda_{seed} = 269$ nm, $\Delta\lambda_{seed} = 3.9$ nm (FWHM) and $\Delta I_{seed} = 1.0$ ps (FWHM).

High quality and stable electron beams. And now?

1. For application: wall plug efficiency and higher repetition rates (1 Hz to 1 kHz, e.g. KALDERA @ DESY)
2. Study plasma physics ;)

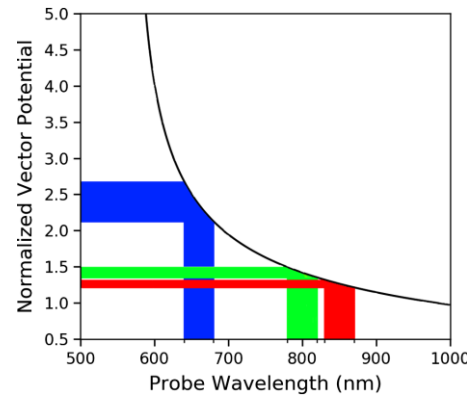
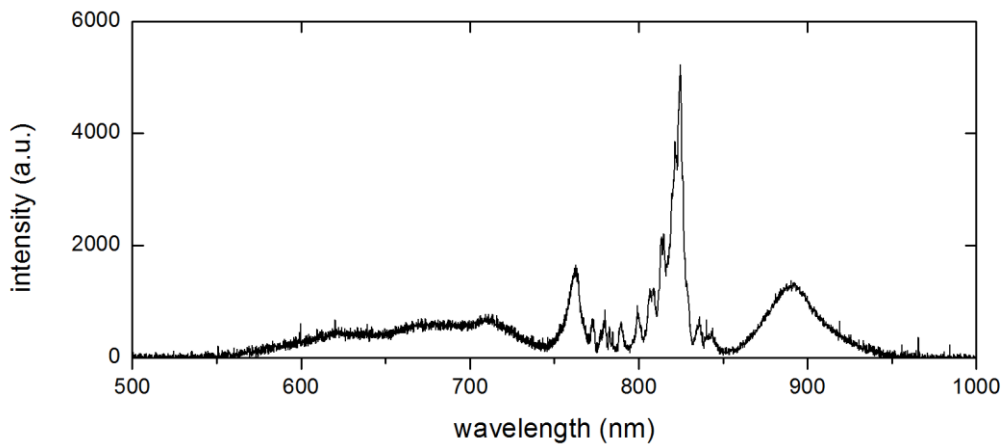
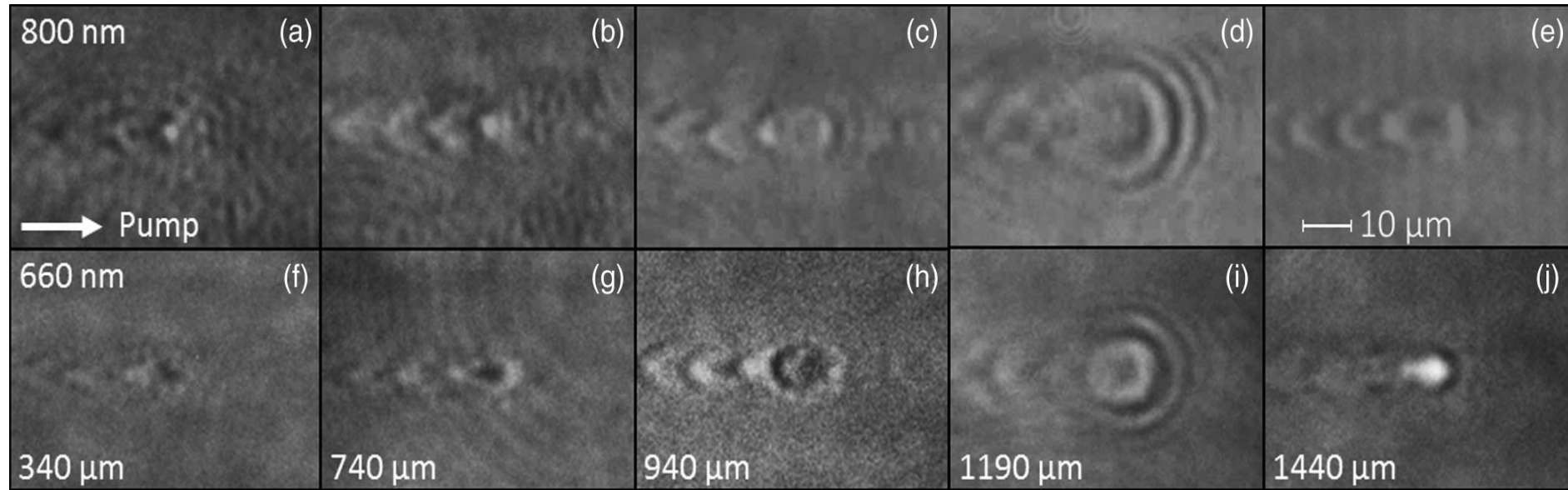
Few Cycle Microscopy - diagnostics



Interferometer

2-channel system
(shadowgraphy, polarimetry,
temporal filtering)

Electron cyclotron resonances in LWFA

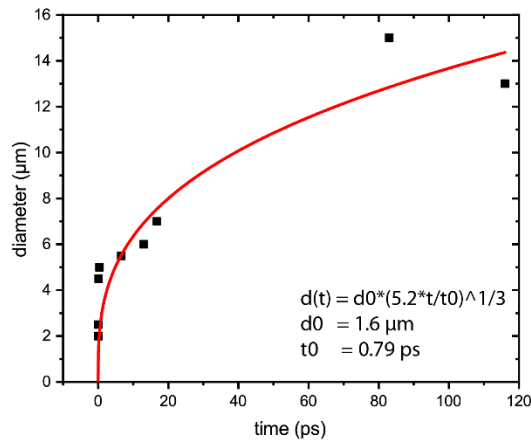
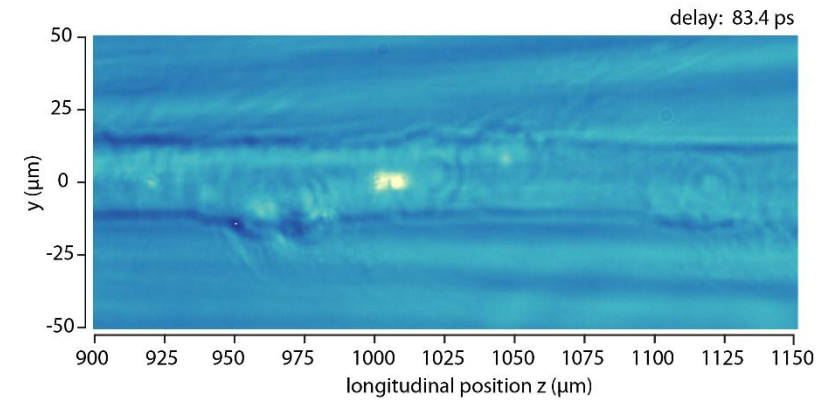
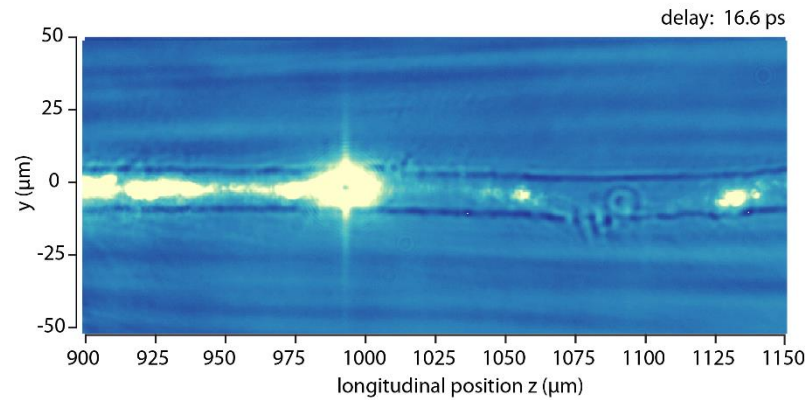
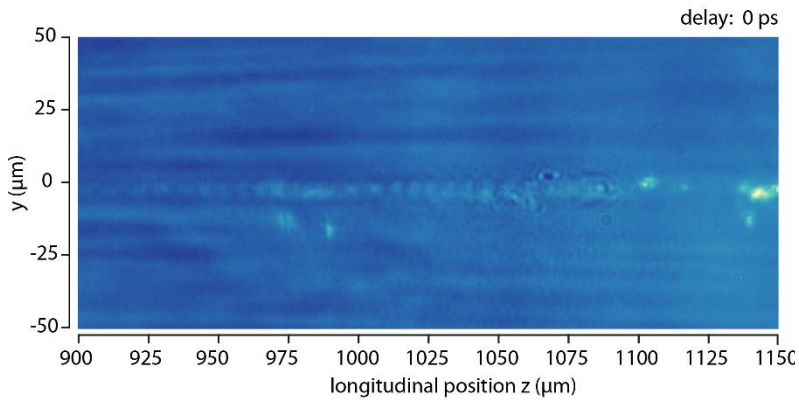


- Magnetic field has substantial contribution to refractive index + additional resonances (polarization dependent)
- visualizing of relativistic laser pulses

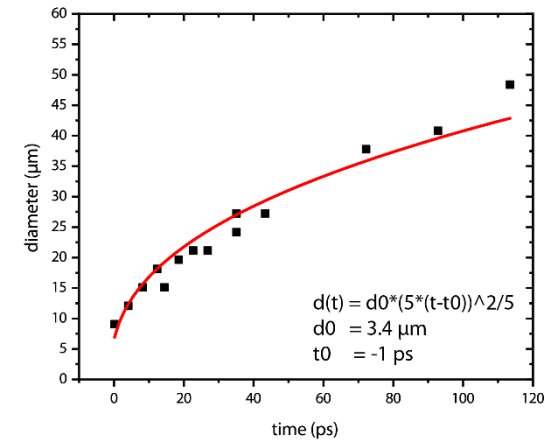
$$\Omega_{ce} = \frac{eB}{\gamma m_e} \quad B \approx a_0 \cdot 11 \text{ kT}$$

Temporal evolution of relativistic postsolitons and plasma channels

A post soliton is a slowly expanding cavity in the ion and electron densities and can emit coherent synchrotron radiation



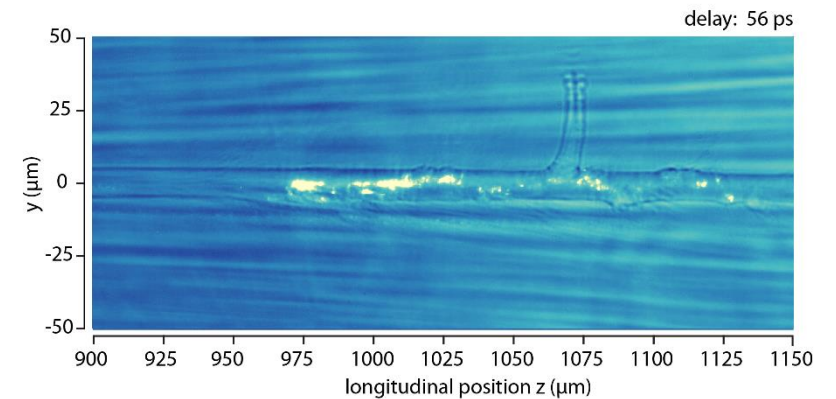
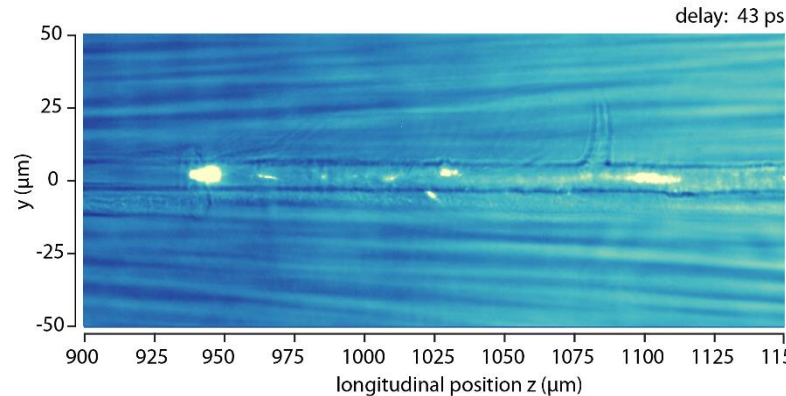
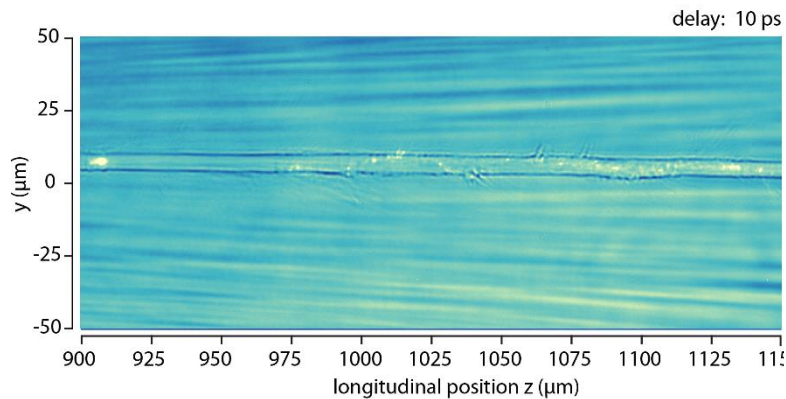
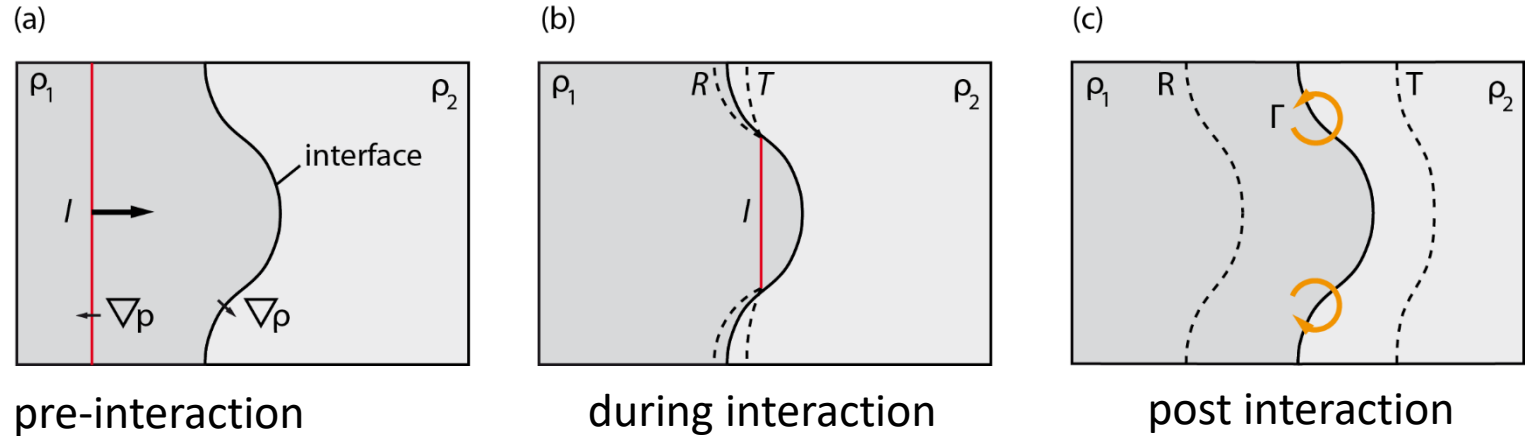
Expansion of the postsolitons in spherical geometry follows a cubic root power law.



Expansion of the plasma channel in cylindrical geometry follows to the power of 2/5.

Richtmyer-Meshkov instability

Richtmyer-Meshkov instability (RMI) is a type of Rayleigh-Taylor instability and generated when a shock wave refracts through the interface between two materials.



Formation of mushroom shaped structures with expansion velocity $v > 4.7 \mu\text{m}/\text{ps}$ i.e. $0.017c$ after the shock passes the boundary of the plasma channel.

Summary & Outlook

- Few Cycle Microscopy gives access to a wide range of plasma phenomena on different timescales
- Allows a direct comparison to simulations
- Electron beams from laser-plasma accelerators nowadays have sufficient beam quality to drive an FEL
- Machine Learning strategies improve day-to-day usage and long term stability